Volcano-Type Correlation between Particle Size and Catalytic Activity on Hydrodechlorination catalyzed by AuPd Nanoalloy

Yuta Uetake,† Sachi Mouri,† Setsiri Haesuwannakij,† Kazu Okumura,‡ Hidehiro Sakurai†,*

†*Division of Applied Chemistry, Graduate School of Engineering, Osaka University, 2-1 Yamadaoka, Suita, Osaka 565-0871, Japan*

‡*Department of Applied Chemistry, Faculty of Engineering, Kogakuin University, 2665-1 Nakano-machi, Hachioji, Tokyo 192-0015, Japan*

ABSTRACT: Although changing the size of metal nanoparticle (NP) is a reasonable way to tune and/or enhance their catalytic activity, size-selective preparation of NP possessing random-alloy morphology has been challenging because of the differences in the ionization potential of each metal ion. This study demonstrates a time-controlled aggregation–stabilization method for a size-selective preparation of random alloy NPs composed of Au and Pd, which are stabilized by poly(*N*-vinyl-2-pyrrolidone) (PVP). By adjusting the mixing time in the presence of a small amount of PVP, the aggregation was induced to produce AuPd:PVP with sizes ranging between 1.2 and 8.2 nm at approximately 1 nm intervals. Transmission electron microscopy (TEM), powder X-ray diffraction (PXRD), and extended x-ray absorption fine structure (EXAFS) analyses clearly

indicated the formation of various sizes of AuPd nanoalloys with almost the same morphology, and size-dependent catalytic activity was observed when hydrodechlorination of 4-choroanisole was performed using 2-propanol as a reducing agent. AuPd:PVP with a size of 3.1 nm exhibited the highest catalytic activity. A comparison of the absorption edges on x-ray absorption near edge structure (XANES) spectra suggested that the electronic state of the Au and Pd species correlated with their catalytic activity, presumably affecting the rate-determining step.

1. INTRODUCTION:

Over the past decade, bimetallic alloy NPs have attracted considerable attention in a wide range of research fields related to heterogeneous catalysts because of their unique catalytic activities.[1] Besides enhancing the catalytic performance of one side of metal species by another counterpart, the most fascinating aspect of alloy effects is their novel catalytic activity, which monometallic NPs do not exhibit.[2] Our early findings of "alloy-specific" reactions on fine chemical synthesis, such as low-temperature Ullmann coupling reaction[2a] and hydrodechlorination[2e] of aryl chloride using *quasi*-homogeneous AuPd bimetallic nanoalloy catalysts, demonstrated its uniqueness. Shishido's group also reported hydrosilylation of 1,4-unsaturated ketone using AuPd nanoalloy catalysts stabilized on solid support.[2g] Since the perturbation of each metal species leads to a drastic change in the electronic structure and surface geometry of NPs (the so-called, ligand effect and ensemble effects),[3] one of the facile ways to tuning the catalytic activity would be the changing the ratio of metal species.[2b,g] Additionally, the interfacial interaction between metal NP and stabilizing agents, such as solid support and polymer matrix, is another way to control the activity,[4] however, few options are available and a novel method to control the catalytic activity of alloy

NPs is required. Since the catalytic activity of metal NPs is strongly affected by their cluster sizes,[5] the development of a method for size-controlled preparation of metal NPs is a promising way to control their catalytic activity. So far, we have established methods for size-selective preparation of AuNPs using poly(*N*-vinyl-2-pyrroridone) (PVP) as a stabilizing matrix.[6] The thus-prepared Au:PVP catalysts were applied for an aerobic oxidation of benzyl alcohol to reveal that the catalytic activity is influenced by the particle size, and also the polymer chain length of PVP (*e.g.* morphology of PVP).[7] Unlike single metal NPs, however, the conventional seed-growth method using small seed NPs and weak reducing agents[6b] is difficult to apply in the case of a bimetallic alloy system due to large differences in the ionization potential of each metal ion source. Hence, size-selective fabrication of metal nanoalloys is one of the challenges in the field of nanometal science, and a new strategy is required to realize it. Here, we describe a time-controlling strategy for a size-selective preparation of AuPd nanoalloys protected by PVP, and discuss their size-dependent catalytic effect on hydrodechlorination.

2. EXPERIMENTAL SECTION

2.1. Modified procedure for the preparation of AuPd:PVP by liquid-phase reduction method. AuPd:PVP with a cluster size of 2.8 ± 1.2 nm was prepared as previously described with minor modification.[2a] To a test tube (Φ = 30 mm), containing PVP(K-30) (278 mg, 2.50 mmol as a monomer unit), water (44 mL), and a magnetic stir bar, was added aqueous $HAuCl_4$ solution (12.5 μmol) and aqueous H_2PdCl_4 solution (12.5 μmol) at 27 °C with stirring at 1300 rpm. After stirring for 5 min, a freshly prepared aqueous solution of $NaBH_4$ (50 mmol/L, 5.0 mL, 0.25 mmol) was added to the mixture in one portion. After stirring for 1 h at the same temperature, the resulting hydrosol was transferred to the ultrafiltration unit (Vivascience, Vivaspin® 20, MWCO: 10,000) using cold water, and concentrated by centrifugal ultrafiltration at 5 °C. After repeating the washing process (ca. 20 mL × 3), the residue was freeze-dried for at least two days to give AuPd:PVP.

2.2. Preparation of AuPd:PVP by microflow module. AuPd:PVPs with cluster size of 1.2 ± 0.4 nm was prepared according to the literature procedure with minor modification[8]: A flow microreactor system consisting of an ultrafine multichannel microfluidic mixer (Toshiba Machine Co., Ltd.) with PTFE tubes (Φ = 0.96 mm) was used. The microflow system and a 100 mL Erlenmeyer flask were immersed in ice water.

In each of the two 50 mL beakers, PVP(K-30) (139 mg, 1.25 mmol as a monomer unit) was dissolved with cold water (25 mL) under irradiation of ultrasound, and both of them were kept cooling with ice water. To one of them were added aqueous $HAuCl_4$ solution (12.5 μmol) and aqueous H_2PdCl_4 solution (12.5 μmol), and the mixture was gentry agitated. The resulting solution was transferred into a plastic syringe (50 mL, 30 mm ID), and this was connected with a plastic

tube and attached on a syringe driver. To the other was added $NaBH_4$ (10 mg, 0.25 mmol) and the mixture was gentry agitated. The resulting solution was transferred into a plastic syringe (20 mL, 30 mm ID), and this was connected with a plastic tube and attached on a syringe driver. The syringe drivers were immediately activated to start flowing at the same moment at the flow rate of 16 mL/min, respectively. The initial small volume was collected into another vial. After confirming the color change of effluent from pale brown to dark brown, the fraction containing AuPd:PVP was collected into the cooled Erlenmeyer flask until when the remaining solution volume reaches 2 mL. The remaining solution was collected into another vial. The resulting hydrosol was transferred to the ultrafiltration unit (Vivascience, Vivaspin® 20, MWCO: 10,000) using cold water, and concentrated by centrifugal ultrafiltration at 5 °C. After repeating the washing process (ca. 20 mL × 3), the residue was freeze-dried for at least two days to give AuPd:PVP.

2.3. Preparation of AuPd:PVP by time-controlled aggregation–stabilization method. To a test tube (Φ = 30 mm), which contains PVP(K-30) (8 mg, 75 μmol as a monomer unit), water (35 mL), and a magnetic stir bar, was added aqueous $HAuCl_4$ solution (12.5 μmol) and aqueous H_2PdCl_4 solution (12.5 μmol) at 27 °C with stirring at 1300 rpm. After stirring for 5 min at the same temperature, a freshly prepared aqueous $NaBH_4$ solution (50 mmol/L, 5.0 mL, 0.25 mmol) was added to the mixture in one portion. After stirring for a specific interval (<1, 20, 60, 180, and 300 s) at the same temperature, to this was added a solution of PVP(K-30) (270 mg, 2.43 mmol as a monomer unit) in H_2O (5 mL). After stirring for 30 min at the same temperature, the resulting hydrosol was transferred to the ultrafiltration unit (Vivascience, Vivaspin® 20, MWCO: 10,000) using cold water, and concentrated by centrifugal ultrafiltration at 5 °C. After repeating the washing process (ca. 20 mL × 3), the residue was freeze-dried for at least two days to give

AuPd:PVP (2.1–3.8 nm). The relationship between cluster size and interval is summarized in Table 1.

Table 1. A scheme of time-control aggregation–stabilization and relationship between aging time and particle size

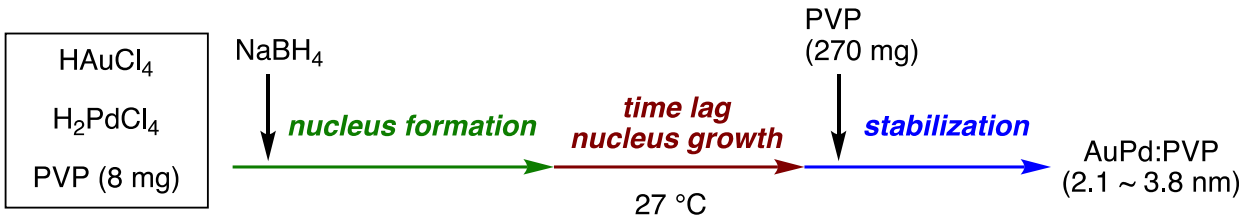

aging time (s)	<1	20	60	180	300
particle size (nm)	2.1 ± 0.6	3.0 ± 1.2	3.1 ± 1.2	3.3 ± 1.2	3.8 ± 1.3

2.4. Preparation of AuPd:PVP by time-controlled aggregation–stabilization method using microflow module. A flow microreactor system consisting of two T-shaped micromixer (Comet X-01, Techno Applications Co., Ltd.) and PTFE tubes (Φ = 0.96 mm) was used (Table 2). Several lengths of silicon tube, which connect between two micromixers, were used to control the time lag for aggregation. The relationship between tube length and time lags were summarized in Table 2. The whole microflow system and a 100 mL Erlenmeyer flask were immersed in ice water.

In a 50 mL beaker, PVP(K-30) (270 mg, 2.43 mmol as a monomer unit) was dissolved with cold water (10 mL) under irradiation of ultrasound, and the mixture was transferred into a plastic syringe (20 mL, 30 mm ID), and this was connected with a plastic tube and attached on a syringe driver (**SD-a**). The flow rate **SD-a** was set at 40 mL/h. In a test tube (Φ = 30 mm) equipped with a magnetic stir bar, PVP(K-30) (8 mg, 75 μmol as a monomer unit) was dissolved with cold water

(25 mL) under the irradiation of ultrasound, and the solution was kept cooling with ice water. To this were added aqueous $HAuCl_4$ solution (12.5 μmol) and aqueous H_2PdCl_4 solution (12.5 μmol), and the mixture was stirred for 5 min. The resulting solution was transferred into a plastic syringe (50 mL, 30 mm ID), and this was connected with a plastic tube and attached on a syringe driver (**SD-b**). The flow rate of **SD-b** was set at 100 mL/h. To a small beaker were added $NaBH_4$ (10 mg, 0.25 mmol) and cold water (5 mL), and the mixture was agitated. The freshly prepared $NaBH_4$ solution was transferred into a plastic syringe (20 mL, 30 mm ID), and this was connected with a plastic tube and attached on a syringe driver (**SD-c**). The flow rate of **SD-c** was set at 25 mL/h. Then, **SD-c** was immediately activated to start flowing. After flowing 0.5 mL of $NaBH_4$ solution, **SD-b** was activated. After activation of **SD-c** for [time lag + 20] s, **SD-a** was activated. The resulting hydrosol was transferred to the ultrafiltration unit (Vivascience, Vivaspin® 20, MWCO: 10,000) using cold water, and concentrated by centrifugal ultrafiltration at 5 °C. After repeating the washing process (ca. 20 mL × 3), the residue was freeze-dried for at least two days to give AuPd:PVP (4.8–8.2 nm). The relationship between cluster size and interval is summarized in Table 2.

Table 2. A scheme of time-controlled aggregation–stabilization using micro-flow conditions and relationship between tube length, aging time, and particle size

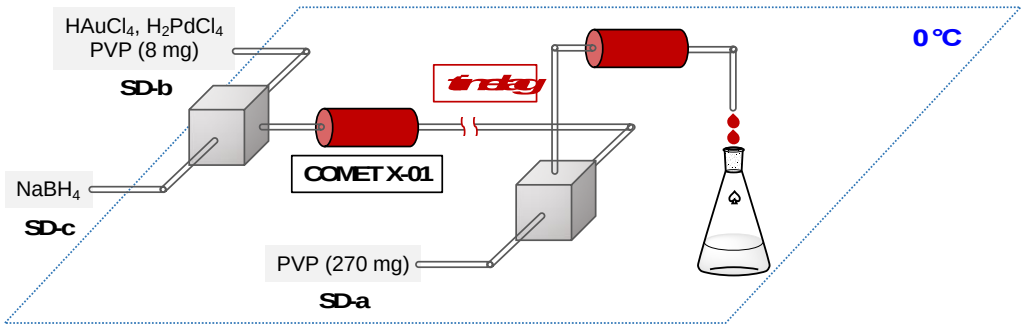

tube length (cm)	6.62	50.8	183	316
aging time (s)	20	60	180	300
cluster size (nm)	4.8 ± 2.1	6.0 ± 2.6	7.1± 3.3	8.2 ± 3.3

2.6. Evaluation of Catalytic Performance. To a flame dried test tube (Φ = 30 mm) equipped with a magnetic stirring bar were added a solution of KOH (16.8 mg, 0.30 mmol) in 2-propanol (2 mL) and 4-chloroanisole (0.2 mmol) under argon atmosphere. After stirring for 5 min at 35 °C, to this was added a solution of AuPd:PVP (2 atom%) in 2-propanol (4 mL). After the specific times, ca. 0.1 mL of the solution was sampled from the mixture using micro syringe to a micro tube. To this were added an aqueous hydrogen chloride solution (ca. 1 mol/L) and water (0.4 mL) immediately, and organic materials were extracted with ethyl acetate (0.5 mL × 3). An aliquot of the solution (0.5 mL) was dispensed into a GC vial, and then to this were added a solution of *n*-hexadecane in ethyl acetate (10 mmol/L, 0.1 mL) and ethyl acetate (0.5 mL). After vigorous mixing using a vortex mixer, GC analysis was carried out using an aliquot of the solution: Constant pressure was adjusted to 115.5 kPa. Temperature of the injection chamber, the column oven, and the flame ionization detector were held at 200, 50 and 280 °C, respectively. The column oven temperature program was set as follows: heated to 100 °C at the rate of 3 °C/min, heated to 280 °C at the rate of 20 °C/min, and held at 280 °C for 2 min. Retention times: anisole (6.9 min), 4-chloroanisole (13.7 min), *n*-hexadecane (22.8 min).

3. RESULTS AND DISOCUSSION

3.1. Size-Selective Preparation of AuPd:PVP and Structural Analyses. Although several studies have reported the effects of alloy NP sizes, they have arguably not evaluated the actual size effects in the true sense due to the presence of other factors, such as extreme differences in particle sizes, different preparation methods, and differences in morphology, which are thought to significantly affect the catalytic activity.[9] To eliminate such an uncertain factors to the greatest possible extent, we decided to use $NaBH_4$ as the sole reducing agent for the size-selective preparation of AuPd:PVP. We began by reinvestigating the conventional liquid-phase reduction. In our previous study on Ullmann coupling reaction, AuPd:PVP(K-30) was prepared using the conventional liquid-phase reduction method with $NaBH_4$ in the presence of equimolar amounts of $HAuCl_4$ and H_2PdCl_4 at 15 °C.[2a] Although monodispersed NPs of an average cluster size of 2.9 ± 0.9 nm were obtained after centrifugal ultrafiltration, Scanning TEM-energy dispersive X-ray spectroscope (STEM-EDX) analysis of the thus-prepared nanoalloy revealed a non-uniform composition of Au and Pd atoms due to the difference in their ionization potentials (Au/Au^{3+} = +1.50 V; Pd/Pd^{2+} = +0.987 V vs. SHE) (Figure S1). To increase the homogeneity of the Au/Pd composition, the temperature of the $NaBH_4$ reduction was optimized to find that at 27 °C, a monodispersed nanoalloy with the similar cluster size (2.8 ± 1.2 nm) was generated reproducibly (Figure 1 and S3). The details of the local structure of Au:Pd:PVP were determined by STEM-EDX and TEM measurements. Judging from the EDX mapping on STEM images, the homogeneity of the nanoalloy's composition was improved compared with that prepared at a lower temperature (Figure S2). High-magnified TEM images revealed that the prepared nanoalloy showed a lattice fringe pattern characteristic of a cubeoctahedron-shaped crystal, with distances of

2.28–2.34 Å, that is, values between those of single Au (2.35 Å, fcc) and Pd NPs (2.25 Å, fcc), also suggesting the formation of a well-mixed nanoalloy (Figure S4).[10,11]

Since it was difficult to obtain the selected area electron diffraction (SAED) image from the nanoalloy due to the weak diffraction intensity of small NPs, next we conducted a survey on the global homogeneity of the nanoalloy using X-ray spectroscopy techniques. Powder X-ray diffraction (PXRD) spectra of AuPd:PVP along with Au:PVP(K-30) and Pd:PVP(K-30) are shown in Figure 2. Although the peaks derived from metal NPs were broadened because of the presence of the polymer matrix surrounding the NPs, the 2θ value of AuPd:PVP was 38–40°, which is the value between those of the Au(111) and Pd(111) facets with fcc crystal structures. Additionally, peaks that can be assigned to the (200) facet were also detected on the shoulder of (111) facet (2θ = 44°) in the case of AuPd:PVP, indicating the fcc crystal structure of the derived nanoalloys.[2a,2g,12] To obtain more information about the alloy structure, X-ray absorption spectroscopy (XAS) measurements at Au L_3- and Pd K-edges were carried out, and the coordination number (CN) and atomic distance of each metal species were analyzed through curve-fitting of *r*-space derived from Fourier transformation of k^3-weighted EXAFS oscillation. In both elements, the shape of the spectra was apparently different from those of the bulk metals, suggesting the formation of an alloy structure (Figure S7,8). Clearer evidence for the alloy structure was obtained from the curve-fitting of the EXAFS spectra, showing the existence of Au–Pd bonding (Table 3). The bond length and CN of Au–Pd, derived from both absorption edges, showed acceptable agreement with each other (Au L_3 edge: 2.78 Å, CN: 3.0; Pd K-edge: 2.77 Å, CN: 4.4), demonstrating the validity of the fitting results. Collated with the CN of monometallic Au NPs with a diameter of 2.8 nm,[7] the sum of the mean CN around the Au atom (8.6) is considered a reasonable value. On the other hand, a relatively small value was observed in the Pd atom (6.5), which indicates that the population of

the existing Pd species is to some extent biased toward the surface of the nanoalloy, reflecting the thermodynamic stability of Au–Au bonding and the intrinsic difference in ionization potential. The bond length of Au–Au was estimated to be 2.79 Å, which is shorter than that of bulk Au (2.85 Å). An extension of the bond length of Pd–Pd (2.78 Å; 2.74 Å for Pd foil) was also observed. These observations are consistent with the experimental results of TEM and PXRD described above. Moreover, almost the same curve-fitting results were derived even with other methods of fabricating AuPd:PVP which are described in the next paragraph (Table 3). Considering all the results, we conclude that AuPd:PVP prepared by liquid-phase reduction using $NaBH_4$ exhibits a random alloy configuration, as revealed by spectroscopic analyses of local and global structures.

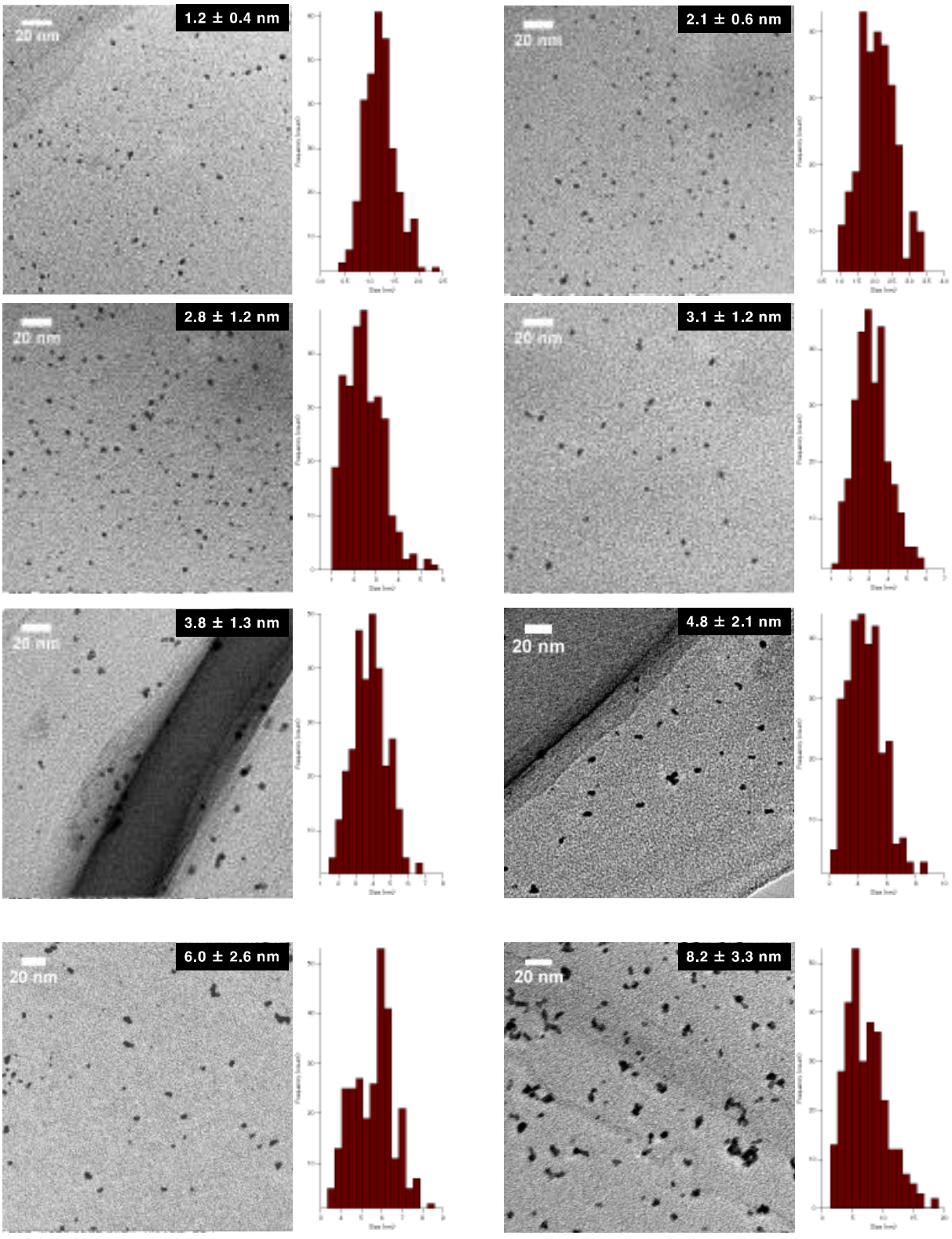

Figure 1. TEM images of AuPd:PVP nanoalloys

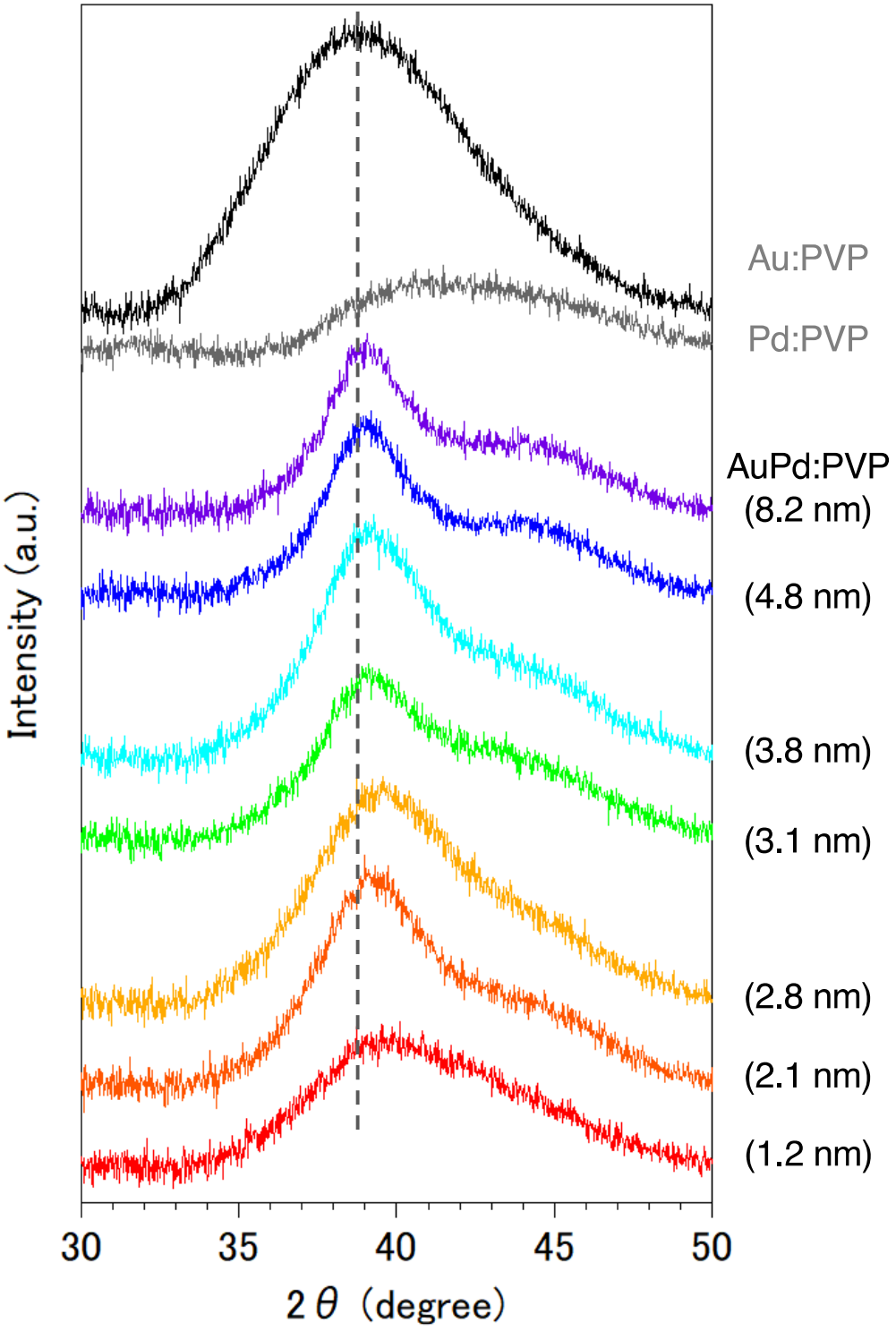

Figure 2. PXRD spectra of Au:PVP, Pd:PVP, and AuPd:PVP NPs

Table 3. Parameters obtained from curve-fitting of Fourier transformed k^3-weighted EXAFS spectra at *r*-space[a]

Particle size (nm)	Shell	CN[b]	R (Å)[c]	ΔE_0 (eV) [d]	σ^2 (10^{-3} Å^2)[e]	$\chi_{\nu 2}$[f]	*R*-factor[g]
2.1	Au–Au	5.6 ± 0.51	2.77 ± 0.007	0.969 ± 1.07	9.48 ± 0.500	18.2	0.0070
	Au–Pd	2.7 ± 0.39	2.75 ± 0.007	6.17 ± 1.05	8.24 ± 0.772		
	Pd–Pd	1.6 ± 0.35	2.77 ± 0.009	–4.17 ± 1.49	6.69 ± 1.20	11.9	0.0027
	Pd–Au	4.4 ± 0.51	2.77 ± 0.008	–4.32 ± 1.33	8.00 ± 0.696		
2.8	Au–Au	5.6 ± 0.61	2.79 ± 0.008	3.14 ± 1.27	10.1 ± 0.631	13.7	0.0085
	Au–Pd	3.0 ± 0.45	2.78 ± 0.007	6.12 ± 1.12	8.56 ± 0.822		
	Pd–Pd	2.1 ± 0.43	2.78 ± 0.010	–2.75 ± 1.43	7.98 ± 1.28	6.3	0.0030
	Pd–Au	4.4 ± 0.58	2.77 ± 0.008	–2.58 ± 1.41	8.22 ± 0.779		
3.1	Au–Au	5.7 ± 0.54	2.78 ± 0.007	2.53 ± 1.11	9.27 ± 0.503	15.1	0.0076
	Au–Pd	3.0 ± 0.42	2.78 ± 0.006	6.40 ± 1.02	7.97 ± 0.746		
	Pd–Pd	2.0 ± 0.64	2.77 ± 0.014	–3.25 ± 2.20	7.22 ± 1.81	12.0	0.0073
	Pd–Au	4.7 ± 0.90	2.77 ± 0.012	–2.64 ± 2.12	8.04 ± 1.09		
3.8	Au–Au	5.5 ± 0.46	2.79 ± 0.006	2.78 ± 0.959	8.67 ± 0.402	18.3	0.0105
	Au–Pd	3.2 ± 0.38	2.79 ± 0.005	6.87 ± 0.859	7.71 ± 0.640		
	Pd–Pd	2.0 ± 0.47	2.77 ± 0.010	–2.59 ± 1.65	6.88 ± 1.35	8.4	0.0038
	Pd–Au	4.5 ± 0.63	2.77 ± 0.008	–4.37 ± 1.58	7.29 ± 0.762		
Au foil	Au–Au	12 (fix)	2.85 ± 0.002	2.77 ± 0.519	8.23 ± 0.202	23.6	0.0037
Pd foil	Pd–Pd	12 (fix)	2.74 ± 0.003	–0.943 ± 0.911	5.52 ± 0.392	543	0.0043

[a]Au L_3: *k*-range = 3–16 Å^{-1}, *r*-range = 1.5–3.3 Å, S_{02} = 0.83 (Au foil); Pd K: *k*-range = 3–14 Å^{-1}, *r*-range: 1.7–3.2 Å, S_{02} = 0.75 (Pd foil). [b]Coordination number. [c]Bond length. [d]Absorption edge energy shift. [e]Debye–Waller factor. [f]Reduced χ-squared value. [g]Goodness-of-Fit index.

In the case of the conventional liquid-phase reduction method, the NP generated *in situ* was immediately stabilized in the presence of an excess amount of PVP (metal ion/PVP = 1:100) before nucleus growth to produce smaller NPs.[6a] To fabricate a larger nanoalloy without using other reducing agents, we expected that an aggregation-induced size growth of nanoalloy would be promoted with a very small amount of stabilizing agent, generating a less stable intermediate

intensively, and that size control could also be achieved by changing the time of the aggregation phase. We began our investigation with these considerations in mind. A solution of $NaBH_4$ (10 equiv) was added to a solution of $HAuCl_4$, H_2PdCl_4, and PVP (3 equiv, as a monomer unit) in H_2O, at 27 °C to generate the nanoalloy. After 300-s aging to promote the aggregation, an excess amount of PVP (97 equiv) was added to stabilize the nanoalloy and cease the aggregation. After the standard purification process, TEM was carried out to ascertain the generation of monodispersed AuPd:PVP with a particle size of 3.8 ± 1.3 nm (n = 3). Next, we investigated the different aging times of the aggregation (<1, 20, 60, and 180 s) in order to control the particle size (Table 2). Although no significant size change occurred until 20 and 60 s, AuPd:PVP with a cluster size of 3.3 ± 1.2 nm was obtained after aging for 180 s. In the case of <1 s aging, a smaller nanoalloy was formed, probably due to the lower initial concentration of PVP, increasing the diffusion rate of the aqueous $NaBH_4$ solution. These results clearly showed that the particle size of the nanoalloy is controllable using the aggregation–stabilization technique. As the mechanism of nucleation is the same as that of the conventional liquid-phase reduction method, the composition of the nanoalloy must be determined at the stage of nucleation and not changed after aggregation. The PXRD spectra and EXAFS analysis of these nanoalloys exhibited almost the same results as in the case of the conventional method, indicating their global uniformity. TEM of the AuPd:PVP (3.1 ± 1.2 nm) was also performed to reveal the local structure. Although some NPs showed the same pattern of lattice fringe as in the case of conventional reduction, a multiply-twinned particles with dodecahedral or regular icosahedral crystal shapes were also observed.[13] A reason for the contamination of crystals with different morphologies may be related to the preparation method of utilizing the aggregation of NP seeds.

In light of the successful experimental results illustrating the concept of aggregation–stabilization, we anticipated that the size-swelling might be achieved by increasing the number of contacts of the NPs, generating much larger nanoalloys. To verify this assumption, a microfluidic reaction condition was applied in order to perform vigorous mixing before the aging phase, facilitating size-growth (Table 2). A COMET X-01 micromixing unit (Techno Applications Co., Ltd.), which is composed of a T-shaped channel controlling unit connected to a double-lane PTFE tube and micromixer,[6c] was chosen for this purpose. Maintaining a constant flow rate, the aging time was controlled by changing the channel length to 6.62, 50.8, 180, and 300 cm, which corresponded to 20, 60, 180, and 300 s, producing AuPd:PVPs with cluster sizes of 4.8 ± 2.1, 6.0 ± 2.6, 7.1 ± 3.3, and 8.2 ± 3.3 nm, respectively. TEM revealed the shape of the nanoalloy to be a polycrystal consisting of cubeoctahedron-shaped crystals, which also reflected the preparation method.

3.2. Catalytic Activity. We previously reported hydrodechlorination of aryl chloride at ambient temperature in the presence of AuPd:PVP nanoalloy using 2-PrOH as a solvent and reducing agent.[6e] With the different methods of size-selective preparation of AuPd:PVP in this study, a survey on the size dependency of the catalytic effect on hydrodechlorination was conducted using 4-chloroanisole as a substrate. Nakajima *et al.* previously reported the preparation of ultra-small AuPd:PVP (ca. 0.9 nm) using an ultrafine multichannel microfluidic mixer originally developed by them.[8] For the sequential survey on the size-dependence of the catalytic activity and electronic structure, their method was applied with minor modifications to fit our preparation conditions, successfully giving AuPd:PVP(K-30) (1.2 ± 0.4 nm). The reaction was performed at 35 °C in all cases to afford anisole as the sole product, and the rate constant (k) and reaction order (n) of each

nanoalloys were derived from the curve-fitting of the time course plot of $1/[A]_{n-1}$ using an *n*- order kinetic equation (Table 4, Figure S9–17). For the sake of comparison, the *k* values were normalized by the surface areas of the corresponding nanoalloys by assuming the spherical shapes with the diameters, and expressed as values divided by that of the smallest nanoalloy (1.2 nm). As a result, the differences in catalytic activity and reaction profile were observed in relation to the particle size. The normalized rate constant (k_{norm}) revealed its maximum value when AuPd:PVP of 3.1 nm was used, and exhibited the so-called "volcano" type of activity profile (Figure 3).[5] Although it has been well recognized that smaller NPs tend to exert better catalytic activity due to the greater number of catalytically reactive sites (i.e. corner and/or edge geometry), size-specific characteristics were observed in this case, probably indicating a significant effect of the electronic structure. Moreover, the reaction order became larger as the particle size increased, suggesting the existence of multiple oxidative added species on the surface of the nanoalloy before the rate determining step.

Table 4. Size-dependent catalytic activity on hydrodechlorination of 4-chloroanisole

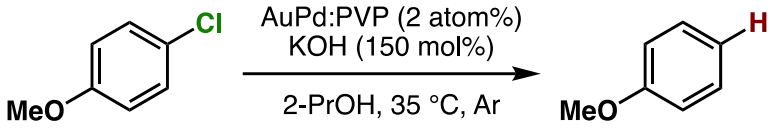

entry	cluster diameter (nm)	colloid size (nm)[a]	k (h^{-1})[b]	k_{normc}	n[b]
1	1.2	131 ± 30	1.78	1	1.1
2	2.1 ± 0.6	111 ± 16	1.11	1.1	1.1
3	2.8 ± 1.2	94 ± 24	1.85	2.4	1.2
4	3.1 ± 1.2	58 ± 18	2.77	4.0	1.2
5	3.8 ± 1.3	68 ± 11	1.34	2.4	1.7
6	4.8 ± 2.1	72 ± 12	0.907	2.0	1.6
7	6.0 ± 2.6	62 ± 11	0.388	1.1	1.8
8	8.2 ± 3.3	103 ± 17	0.233	0.89	2.4

[a]Induced grating (IG) method (0.3 mmol/L for PVP). [b]Derived from the curve-fitting using the equation of $1/[A]_{n-1} = (n-1)kt + 1/[A]_{0n-1}$ ([A]: concentration of 4-chloroanisole, t: time (h)); [c]$k_{norm} = (k_m \times d_m)/(k_1 \times d_1)$, $k_1 = 1.2$, $d_1 = 1.78$.

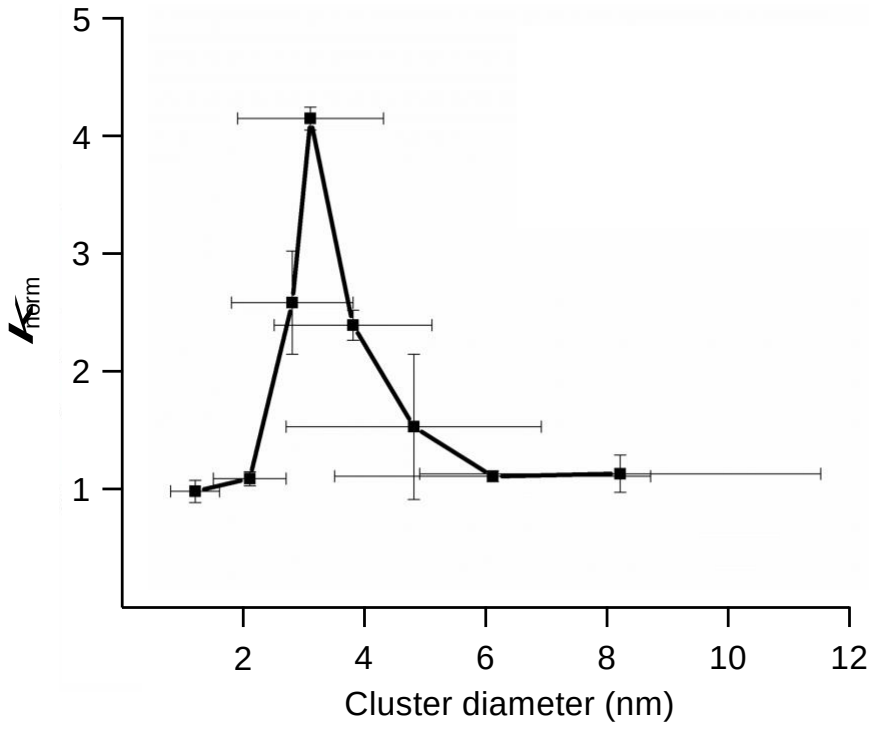

Figure 3. Correlation between particle size and normalized rate constant

3.3. Analyses of Electronic State and Interfacial Morphology. To elucidate the relationship between particle size and the electronic state of the prepared AuPd:PVPs with several particle sizes, precise XANES analyses were carried out. The shape of XANES spectra of AuPd:PVP are quite resemble each other in both absorption edges, which indicated that these Au NPs possess similar density of state.[14–16] The Au L_3-edge XANES spectra showed a less intense white line signal, suggesting the probability of electronic dipolar transition from the $2p_{3/2}$ to the 5*d* band, which was attributed to charge transfer from Pd atoms and PVP.[7a] The lowest intensity was observed in the case of AuPd:PVP with a diameter of 3.1 nm, which exhibited the highest catalytic activity (Figure 4). Pd K-edge XANES analysis also revealed that AuPd:PVP with a diameter of 3.1 nm showed the highest absorption edge energy, indicating the formation of electron-deficient Pd species, attributed to the electron-withdrawing effect of the electron-negative Au atoms. Regarding the electronic state of these two metals, the results of XANES spectra at both edges correlated with each other, indicating not only that the electron-rich Au and electron-deficient Pd species might affect to the catalytic activity but also that the electronic state of the nanoalloy is perturbated only by changing the cluster size. The colloid sizes in an aqueous solution were also estimated using induced grating (IG) method to clarify the interfacial morphology between the surrounding PVP and the core metal (Table 4).[7b] The smallest colloid size (58 ± 18 nm) was observed in the case of the 3.1 nm cluster size, indicating a strong interaction between the metal surface and the PVP matrix. In our research into the "matrix effect of PVP", we found that the electronic state on the metal surface correlates with the colloid size, probably due to proximity-enhanced electron-donation from carbonyl groups of PVP to the core metal.[7] Although in this case, it is difficult to clarify the role of PVP because of the additional electronical influence of the adjacent Au species,

we assumed that electron-donation from PVP might facilitate the oxidative addition step. The origin of the size-dependent catalytic activity remains unclear due to the multiple factors, such as the quantum size effect, the composition of metal surface (so-called ensemble effect), and the interfacial morphology, in addition to the issues described above. Therefore, more precise experimental and theoretical investigations are required.

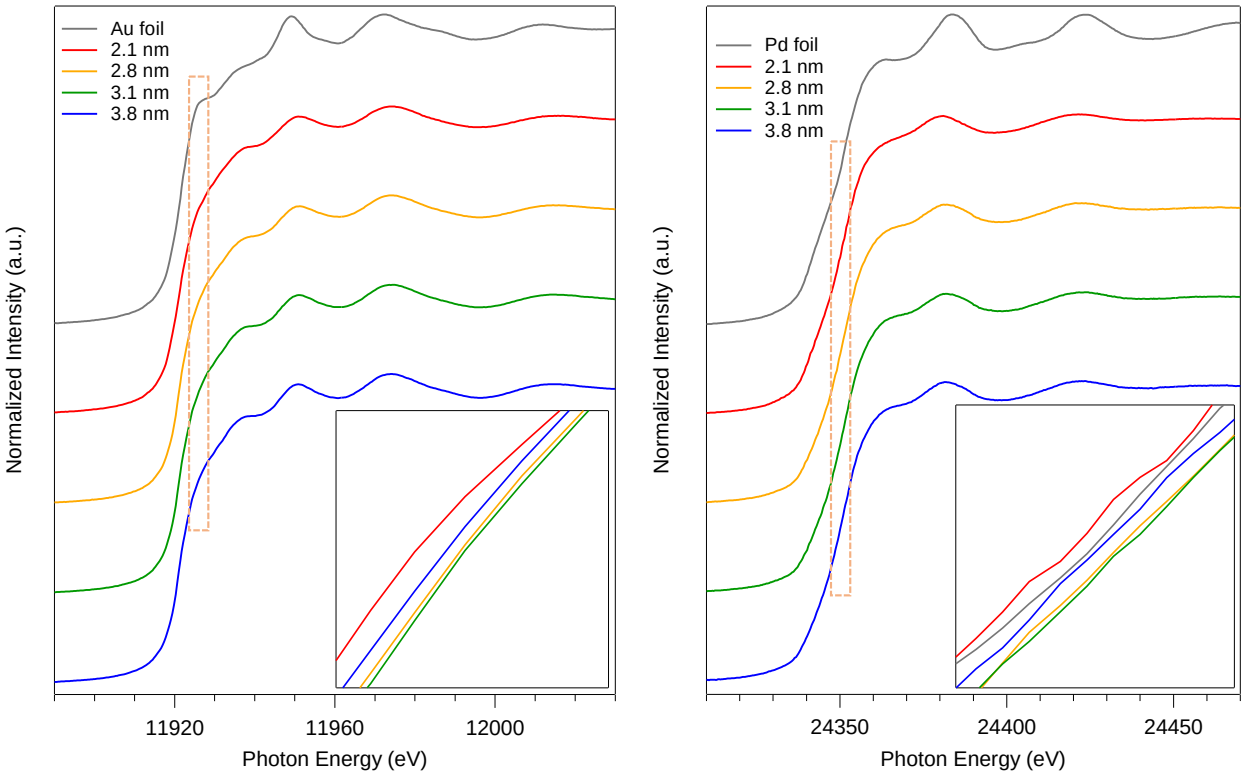

Figure 4. Au L_3- and Pd K-edge XANES spectra of AuPd:PVP (2.1, 2.8, 3.1, and 3.8 nm) and these magnifications at the absorption edge.

4. CONCLUSION

We achieved a size-controlled preparation of AuPd nanoalloy protected by PVP with a precision of approximately 1-nm intervals based on the time-controlled aggregation–stabilization technique. Thanks to the use of the same reducing agent, different sizes of AuPd:PVP with almost the same morphology were furnished, allowing us to thoroughly investigate the size-dependent catalytic activity. AuPd:PVP with a size of 3.1 nm showed the highest catalytic effect on hydrodechlorination of 4-chloroanisol. The employed methods are quite practical because of the easy preparation protocol, and enabled us to observe new phenomena. Furthermore, in combination with the trans-deposition method developed by our group,[17] it may possible to prepare a size-determined AuPd nanoalloy deposited on solid support with retaining its cluster size, thus broadening its range of applications.

ASSOCIATED CONTENT

Supporting Information.

The Supporting Information is available free of charge at http://xxx.

Experimental procedures; magnified TEM and STEM-EDX images; EXAFS spectra; experimental data for kinetics (PDF).

AUTHOR INFORMATION

Corresponding Author

*E-mail: hsakurai@chem.eng.osaka-u.ac.jp

ORCID

Yuta Uetake: 0000-0002-4742-8085

Kazu Okumura: 0000-0002-7952-3482

Hidehiro Sakurai: 0000-0001-5783-4151

Notes

The authors declare no competing financial interest.

ACKNOWLEDGMENT

This work was supported by JSPS-KAKENHI (JP19K22187) and JST(ACT-C) Project (JPMJCR12YI). STEM-EDX measurements at Osaka University were supported by "Nanotechnology Platform Program" of the Ministry of Education, Culture, Sports, Science and Technology (MEXT), Japan. XAS measurements were performed at BL01B1 at SPring-8 with the approval of the Japan Synchrotron Radiation Research Institute (JASRI) (Proposal No. 2015A1134, 2016B1148).

REFERENCES

(1) (a) Toshima, N.; Yonezawa, T. *New J. Chem.* **1998**, *22*, 845–910. (b) Ferrando, R.; Jellineck, J.; Johnston, R. L. *Chem. Rev.* **2008**, *108*, 845–910. (c) Nørskov, J. K.; Bligaard, T.; Rossmeisl, J.; Christensen, C. H. *Nat. Chem.* **2009**, *1*, 37–46.

(2) (a) Dhital, R. N.; Kamonsatikul, C.; Somsook, E.; Bobuatong, K.; Ehara, M.; Sakurai, H. *J. Am. Chem. Soc.* **2012**, *134*, 20250–20253. (b) Murugadoss, A.; Okumura, K.; Sakurai, H. *J. Phys. Chem. C* **2012**, *116*, 26776–26783. (c) Dhital, R. N.; Kamonsatikul, C.; Somsook, E.; Sakurai, H. *Catal. Sci. Technol.* **2013**, *3*, 3030–3035. (d) Dhital, R. N.; Bobuatong, K.; Ehara, M.; Sakurai, H.

Chem. Asian J. **2015**, *10*, 2669–2676. (e) Karanjit, S.; Jinasan, A.; Somsook, E.; Dhital, R. N.; Motomiya, K.; Sato, Y.; Tohji, K.; Sakurai, H. *Chem. Commun.* **2015**, *51*, 12724–12727. (f) Agarwal, N.; Freakley, S. J.; McVicker, R. U.; Althahban, S. M.; Dimitratos, N.; He, Q.; Morgan, D. J.; Jenkins, R. L.; Willock, D. J.; Taylor, S. H.; Kiely, C. J.; Hutchings, G. J. *Science* **2017**, *358*, 223–227. (g) Miura, H.; Endo, K.; Ogawa, R.; Shishido, T. *ACS Catal.* **2017**, *7*, 1543–1553. (h) Miura, H.; Sasaki, S.; Ogawa, R.; Shishido, T. *Eur. J. Org. Chem.* **2018**, 1858–1862. (i) Miura, H.; Tanaka, Y.; Nakahara, K.; Hachiya, Y.; Endo, K.; Shishido, T. *Angew. Chem., Int. Ed.* **2018**, *57*, 6136–6140. (j) Williams, C.; Carter, J. H.; Dummer, N. F.; Chow, Y. K.; Morgan, D. J.; Yacob, S.; Serna, P.; Willock, D. J.; Meyer, R. J.; Taylor, S. H.; Hutchings, G. J. *ACS Catal.* **2018**, *8*, 2567–2576. (k) Nakajima, K.; Tominaga, M.; Waseda, M.; Miura, H.; Shishido, T. *ACS Sustainable Chem. Eng.* **2019**, ***7***, 6522–6530. (l) Sadhukhan, T.; Junkaew, A.; Zhao, P.; Miura, H.; Shishido, T.; Ehara, M. *Organometallics* **2020**, *39*, 528–537. (m) Miura, H.; Masaki, Y.; Fukuta, Y.; Shishido, T. *Adv. Synth. Catal.* **2020**, 362, 2641–2650.

(3) Cao, S.; Tao, F.; Tang, Y.; Li, Y.; Yu, J. *Chem. Soc. Rev.* **2016**, *45*, 4747–4765.

(4) (a) Walsh, T. R.; Knecht, M. R. *Chem. Rev.* **2017**, *117*, 12641–12704. (b) Heuer-Jungemann, A.; Feliu, N.; Bakaimi, I.; Hamaly, M.; Alkilany, A.; Chakraborty, I.; Masood, A.; Casula, M. F.; Kostopoulou, A.; Oh, E.; Susumu, K.; Stewart, M. H.; Medintz, I. L.; Stratakis, E.; Parak, W. J.; Kanaras, A. G. *Chem. Rev.* **2019**, *119*, 4819–4880. (c) Sanker, M.; He, Q.; Engel, R. V.; Sainna, M. A.; Logsdail, A. J.; Roldan, A.; Willock, D. J.; Agarwal, N.; Kiely, C. J.; Hutchings, G. J. *Chem. Rev.* **2020**, *120*, 3890–3938.

(5) (a) Valden, M.; Lai, X.; Goodman, D. W. *Science* **1998**, *281*, 1647–1650. (b) Liu, Y.; Tsunoyama, H.; Akita, T.; Xie, S.; Tsukuda, T. *ACS Catal.* **2011**, *1*, 2–6.

(6) (a) Tsunoyama, H.; Sakurai, H.; Negishi, Y.; Tsukuda T. *J. Am. Chem. Soc.* **2005**, *127*, 9374–9375. (b) Tsunoyama, H.; Sakurai, H.; Tsukuda, T. *Chem. Phys. Lett.* **2006**, *429*, 528–532. (c) Haesuwannakij, S.; Karuehanon, W.; Mishra, V. L.; Kitahara, H.; Sakurai, H.; Kanaoka, S.; Aoshima, S. *Monatsh Chem.* **2014**, *145*, 23–28.

(7) (a) Tsunoyama, H.; Ichikuni, N.; Sakurai, H.; Tsukuda, T. *J. Am. Chem. Soc.* **2009**, *131*, 7086–7093. (b) Haesuwannakij, S.; Kimura, T.; Furutani, Y.; Okumura, K.; Kokubo, K.; Sakata, T.; Yasuda, H.; Yakiyama, Y.; Sakurai, H. *Sci. Rep.* **2017**, *7*, 9579.

(8) Hayashi, N.; Sakai, Y.; Tsunoyama, H.; Nakajima, A. *Langmuir* **2014**, *30*, 10539–10547.

(9) Cheng, J.; Gu X.; Sheng, X.; Liu, P.; Su, H. *J. Mat. Chem. A* **2016**, *4*, 1887–1894.

(10) Tsen, C.-S. Y.; Crozier, P. A.; Liu, J. *Ultramicroscopy* **2003**, *98*, 63–72.

(11) Zhang, D.; Jin, C.; Tian, H.; Xiong, Y.; Zhang, H.; Qiao, P.; Fan, J.; Zhang, Z.; Li, Z. Y.; Li, J. *Nanoscale* **2017**, *9*, 6327–6333.

(12) Geraldes, A. N.; Furtunato da Silva, D.; Pino, E. S.; Martin da Silva, J. C.; Brambilla de Souza, R. F.; Hammer, P.; Spinacé, E. V.; Neto, A. O.; Linardi, M.; Coelho dos Santos, M. *Electrochimica Acta* **2013**, *111*, 455–465.

(13) Jian, N.; Palmer, R. E. *J. Phys. Chem. C* **2015**, *119*, 11114–11119.

(14) Marx, S.; Baiker, A *J. Phys. Chem. C* **2009**, *113*, 6191–6201.

(15) Liu, F.; Wechsler, D.; Zhang, P *Chem. Phys. Lett.* **2008**, *461*, 254–259.

(16) (a) Dash, P.; Bond, T.; Fowler, C.; Hou, W.; Coombs, N.; Scott, R. W. J. *J. Phys. CHem. C* **2009**, *113*, 12719–12730. (b) Balcha, T.; Strobl, J. R.; Fowler, C.; Dash, P.; Scott, R. W. J. *ACS Catal.* **2011**, *1*, 425–436.

(17) Haesuwannakij, S.; Poonsawat, T.; Noikham, M.; Somsook, E.; Yakiyama, Y.; Dhtal, R. N.; Sakurai, H. *J. Nanosci. Nanotechnol.* **2017**, *17*, 4649–4657.